



QUANTUM INTERNET ALLIANCE

D2.4 Comparison report on long distance quantum repeater links

Document History

Revision Nr	Description	Author	Review	Date
1	First draft	Hugues de Riedmatten, Samuele Grandi, Mikael Afzelius, Wolfgang Tittel		15.03.2022
2	Revised version	Hugues de Riedmatten, Samuele Grandi, Mikael Afzelius, Wolfgang Tittel		25.03.2022

This project has received funding from the European Union's Horizon 2020 research and innovation programme under grant agreement No 820445.

The opinions expressed in this document reflect only the author's view and in no way reflect the European Commission's opinions. The European Commission is not responsible for any use that may be made of the information it contains.

Index

1. Abstract	5
2. Keyword list	5
3. Acronyms & Abbreviations	5
4. Introduction	6
5. Non-classical correlations and entanglement between fixed storage time quantum memories and telecom photons	7
5.1 Praseodymium quantum memories (ICFO)	7
5.2 Ytterbium quantum memories (UNIGE)	9
5.3 Thulium quantum memories (TUD)	11
6. Non-classical correlations and entanglement between on-demand quantum memories and telecom photons	12
6.1 Emissive quantum memories and quantum frequency conversion	12
6.2 Absorptive quantum memories	16
7. Telecom heralded entanglement between remote solid-state multiplexed quantum memories	18
8. Conclusion	20
9. References	22

1. Abstract

In this report, we describe the progress realized during QIA towards the realization of memory based quantum repeaters. We report significant progress in experiments demonstrating entanglement and non-classical correlations between telecom photons and solid-state quantum memories. We also report the first demonstration of telecom heralded entanglement between multimode quantum memories, which can be in principle extended to long distances.

2. Keyword list

Entanglement, solid-state quantum memory, telecom photons.

3. Acronyms & Abbreviations

DoA	Description of Action
EC	European Commission
WP	Work Package
AFC	Atomic frequency comb
SW	Spin wave
DLCZ	Duan-Lukin-Cirac-Zoller
QFC	Quantum Frequency Conversion
RE	Rare-earth
SPDC	Spontaneous parametric down conversion
EOM	Electro-optic modulator

4. Introduction

WP2 develops the quantum technologies for the realization of quantum repeaters. A crucial building block for quantum repeaters is the generation of entanglement between remote quantum memories. Long distance fiber based entanglement requires the distribution of photons over lossy optical fibers and is therefore a probabilistic process. For the repeater to be scalable, it is necessary that the entanglement within an elementary link is heralded, which means that there must be a signal informing of a successful entanglement generation attempt, and that the entanglement is stored in quantum memories until this signal arrives. To achieve this requirement, the entanglement between the remote quantum nodes is generated by performing a Bell state measurement between photons emitted by the nodes at a central station between the nodes. This projective measurement at the central station heralds the entanglement.

Two techniques can be used for the Bell state measurement: BSM based on one-photon detection, and BSM based on two-photon detection. For the one-photon BSM, the nodes are weakly excited and one telecom photon is created, transmitted and detected at the central station. A successful single photon detection at the central station projects the two quantum memories into an entangled state in the Fock basis, where one collective excitation is stored in coherent superposition between the two remote quantum nodes. In that case, the main figure of merit for the nodes is the quality of the non-classical correlation between the quantum memory and the telecom photon. This strategy has the great advantage to lead to high count rate, but has the drawback that the phase between the nodes and the central station has to be controlled, which represents a significant technical challenge. Each node generates entanglement between the node and a photon at telecom wavelength. The second strategy is based on a two-photon BSM. In that case, each node creates entanglement between the quantum memory and a telecom photon, e.g. using the polarization or time-bin degree-of-freedom. The two telecom photons are then transferred to the central station where a BSM is performed, which projects the two memories into an entangled state. This strategy leads to considerably lower count rates because in that case two photons have to be created, transmitted and detected. However, the phase acquired by the photons between the nodes and the central station is not relevant and the only condition is that the two photons arriving at the central station are indistinguishable. For this second strategy, the main resource is therefore the generation of entanglement between a quantum memory and a telecom photon.

In this deliverable, we describe various experiments done in QIA demonstrating the main resource for the generation of elementary quantum repeater links, namely non-classical correlation or entanglement between quantum memories and telecom photons. In QIA, this capability has been achieved with various fixed storage time solid-state quantum memories based on rare-earth doped solids, e.g. Pr:YSO (ICFO), Yb:YSO (UNIGE) and Tm:YGG (TUD) (section 5). We also report entanglement demonstrations over long distance of optical fibers, including a 50 km long fiber of the standard telecom network in the Barcelona area. In addition, we report entanglement and non-classical correlation demonstrations between telecom photons and spin wave on demand absorptive quantum memories in Pr:YSO (ICFO), as well as the demonstration of sources of correlated and entangled photon pairs using emissive quantum memories in Eu:YSO (UNIGE) and Pr:YSO (ICFO) (section 6). Finally, we report on the creation of telecom heralded entanglement between two solid-state quantum memories based on Pr doped crystals (ICFO), placed in two laboratories separated by 10 m (section 7).

5. Non-classical correlations and entanglement between fixed storage time quantum memories and telecom photons

5.1 Praseodymium quantum memories (ICFO)

ICFO has developed a system for the generation of light-matter entanglement between a telecom photon and a fixed storage time solid-state memory based on praseodymium-doped crystals.

This architecture exploits the combination of different strategies for the generation and the storage of entanglement. For the former, ICFO developed a photon pair source based on cavity-enhanced spontaneous parametric down-conversion. A non-linear crystal of periodically-poled lithium niobate is placed inside an optical cavity, which enhances the generation of photon pairs and at the same time narrows their spectrum to below 2 MHz, making it compatible with solid-state quantum memories. The parametric process is also highly non-degenerate, and leads to the generation of an idler photon in the telecom band and a visible signal photon, at 606 nm, therefore bridging the gap between atomic systems and telecommunication band. Moreover, the spectrum of the photon pairs is actually composed of about 15 separate frequency modes, a precious resource for multiplexing in long-distance quantum communication.

While the idler photon can be sent through telecom fibres over long distances, the signal photon is stored in a solid-state quantum memory. This is a praseodymium-doped crystal that is cooled in a closed-cycle cryostat to 3 K. The population of the Pr ions on the $^3H_4 - ^1D_2$ transition is shaped into a comb-like structure through optical pumping. This is the Atomic Frequency Comb (AFC) protocol¹, and a photon absorbed by the comb on this transition will be re-emitted at a time $\tau_{AFC} = 1/\Delta$, where Δ is the periodicity of the comb in frequency. The AFC protocol is multimode in time, in that single photons can be stored continuously, and will be re-emitted in the same order. At the same time, the system supports frequency multiplexing, since separate AFC can be realised in the inhomogeneous broadening of the Pr ions. We actually implemented such a configuration², storing all the frequency modes generated by the photon pair source, as reported in deliverable D2.2: Report on highly multimode memories.

The setup of the experiment is reported in Fig. 1. This setup is the same used for implementing on-demand read-out from the quantum memory by storing in one of the spin states. We started by characterising the combined system of source and quantum memory by measuring the efficiency of the AFC storage and the cross-correlation function as a function of the storage time in the quantum memory. The results are reported in Fig. 2. By fitting the data of the storage efficiency to the an exponential decay of the form $\exp\left(-4 \frac{\tau}{T_2^{eff}}\right)$ we were able to extract the effective coherence time of

the AFC storage³, as $T_2^{eff} = 92(9) \mu\text{s}$. At the same time, the cross-correlation function is well-above the limit of 2, valid for classical light.

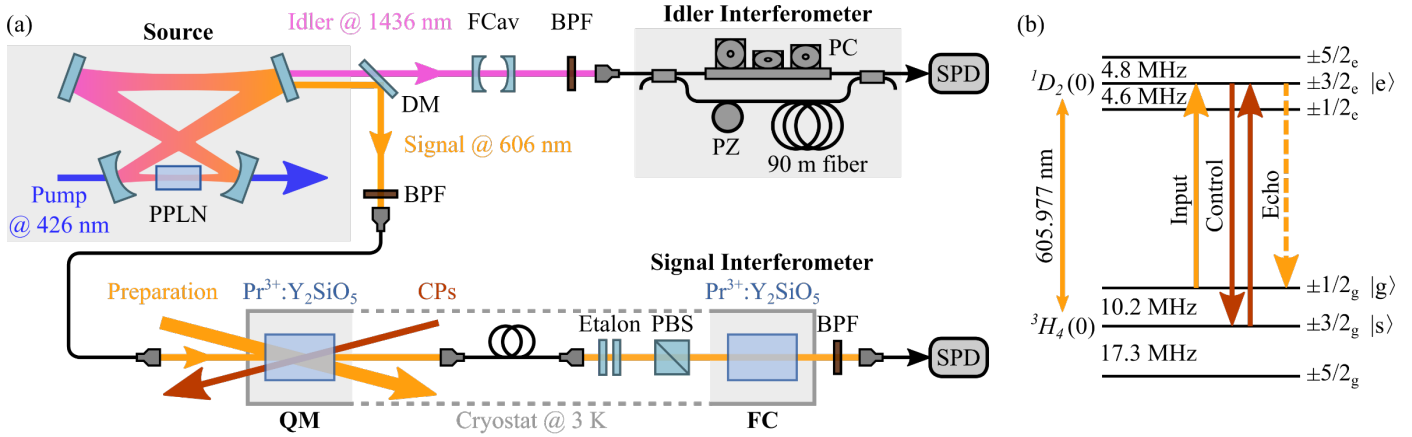


Figure 2: (a) setup of the experiment for the storage and analysis of entanglement between a telecom photon and a solid-state quantum memory. (b) relevant transitions of ³⁺Pr:Y₂SiO₅.

The signal and idler photon are entangled in energy and time, this means that they are emitted at the same time, within the coherence time of the pump laser. The Franson scheme⁴ is used to analyse this type of entanglement, whereby a Mach-Zehnder interferometer is placed at the idler and signal path, and coincidences are measured as a function of the relative phase between the arms of the two interferometers. On the idler side, we placed a fibre-based interferometer, where the difference in length between the short and long arm is 420 ns. For the signal we implemented a solid-state version using another Pr-doped crystal, in which we prepared two AFCs with storage time differing by 420ns, such that a photon had equal probability to be absorbed by either. We selected two values of phase for the idler interferometer, and for each varied the phase of the signal interferometer and measured the idler-signal coincidences⁵. The result is reported in Fig. 3, where the two interference fringes are shown for a storage time in the AFC of 10 μs . The visibility of

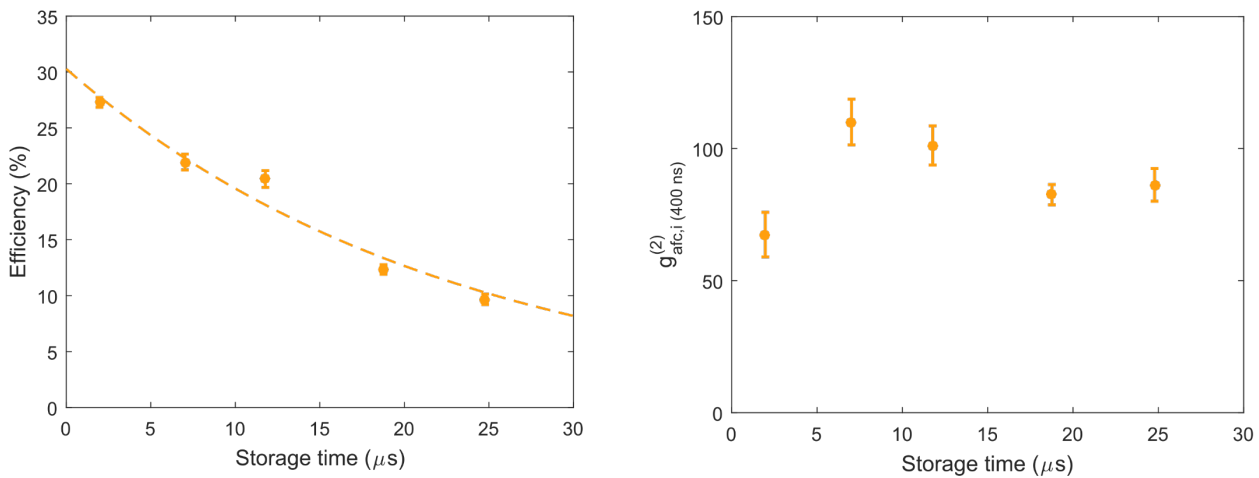


Figure 1: (left) efficiency of the AFC storage as a function of storage time. By fitting the data to an exponential we were able to extract the effective coherence time T_2^{eff} . (right) cross-correlation function of telecom idler photon and retrieved signal photon, for different storage times.

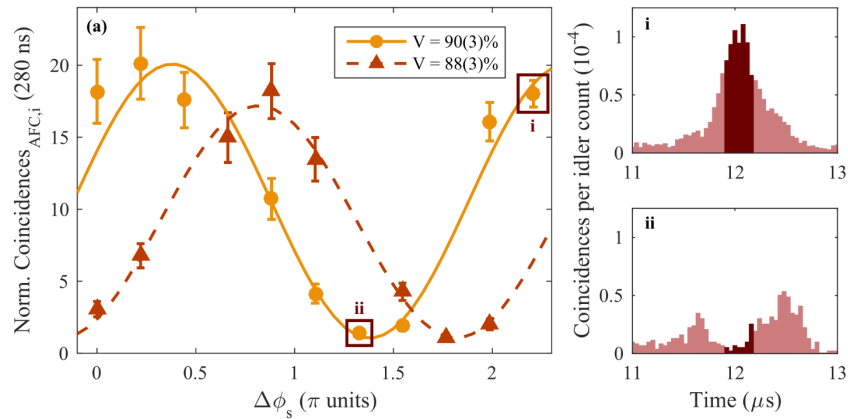


Figure 3: fringes of interference for storage in the excited state. Two coincidence histograms are reported in the side panels.

each one is about 90%, enough to demonstrate a violation of a CHSH inequality and therefore demonstrate the entanglement between the telecom idler photon and the collective excitation of the Pr ions. The corresponding two qubit fidelity is 92 (2) %.

This system, featuring entanglement between a telecom photon and a long-lived collective excitation, is perfectly suited for the long-distance distribution of entanglement. This could be achieved both through heralded entanglement swapping (as will be described in section 7) or through direct transmission. In either case, the storage time should equal the communication time, which is the time required for the idler photon to reach its destination and for the detection signal to come back. The maximum distance allowed by the memory in this configuration is only of a few km. Nonetheless, the entanglement verification can be run in a configuration where the signal photon is re-emitted and detected before the idler photon is. We then connected our system with two fibres of a metropolitan link, connecting ICFO with downtown Barcelona, and spanning about 25 km in length. These two fibres were connected in a loop, such that idler photons traveled 50 km of metropolitan fibre before returning to ICFO. Only preliminary results are available for this measurement, where nonetheless we measured an un-changed cross-correlation function of 61(7) with respect to the experiment performed fully in the lab. We then performed an analysis of the entanglement, and we measured a visibility of 83(6)%, clearly demonstrating remote light-matter entanglement, and fulfilling the milestone M2.9.

5.2 Ytterbium quantum memories (UNIGE)

Ytterbium-doped quantum memories are based on a novel RE material, $^{171}\text{Yb}^{3+}:\text{Y}_2\text{SiO}_5$ (Yb:YSO), following a spectroscopic study from 2018⁶. The key features of this material are long optical and spin coherence times at zero applied magnetic field, owing to all states being “clock” states simultaneously. These properties arise from the completely hybridized electron-nuclear spin states due to an highly anisotropic hyperfine interaction. The main benefit of Yb:YSO for quantum memories lies in the large hyperfine splittings (GHz regime), which in principle should allow broadband quantum memories (eg. as compared to Eu:YSO or Pr:YSO) while still having long storage times owing to

the clock states. A proof-of-principle experiment in 2020 demonstrated a 10-MHz AFC memory⁷, which was still far below the potential bandwidth of at least 250 MHz.

Storage experiments with the SPDC source were made for storage times between $1 \mu\text{s}$ and $25 \mu\text{s}$ and strong non-classical correlations were observed after storage, ranging from $g_{si}^{(2)}(0) = 28(4)$ to $g_{si}^{(2)}(0) = 14(1)$, see Fig. 4. These values are peak values, the values for the full mode are roughly two times lower. The single-photon storage efficiency at $5 \mu\text{s}$ was 4.9%, lower than the classical 15% efficiency observed previously for a lower AFC bandwidth of 10 MHz. The difference is due to the poorer QM-photon bandwidth match (overlap of 60%) and lower optical depth in the AFC due to the lack of laser power when preparing a 100 MHz AFC. The effective AFC coherence time was $T_2^{eff} = 69(6) \mu\text{s}$, about 25% shorter than the value obtained in Pr:YSO. However, in photon echo measurements a coherence time of $800 \mu\text{s}$ has been obtained⁸, showing the potential for increasing the maximum storage time with one order of magnitude, with a correspondingly larger multimode capacity.

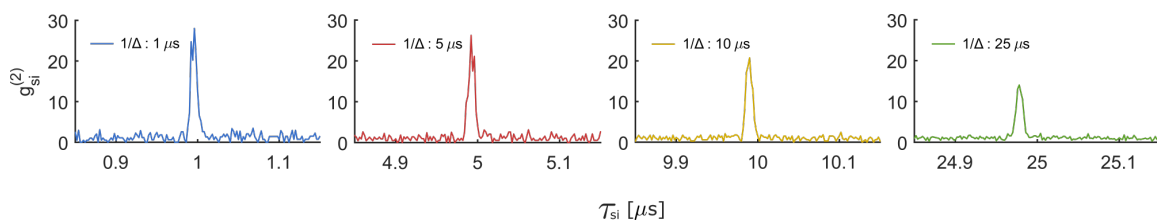


Fig. 4. Second-order cross-correlation $g_{si}^{(2)}$ as a function of signal-idler coincidence delay τ_{si} . The peaks show the preservation of non-classical correlations after storage in a Yb:YSO quantum memory, with storage times ranging from between $1 \mu\text{s}$ to $25 \mu\text{s}$.

The multimode capacity was analyzed in detail for a storage time of $25 \mu\text{s}$, see Fig. 5(a), showing that the rate of the experiment scales linearly with the number of modes, a key feature of multiplexed quantum repeaters. The total number of stored modes were 1250, with clear non-classical correlations across all modes. The storage time allows propagating the telecom photon through a fiber of 5 km, see Fig. 5(b), and still detect the heralding telecom photon before the release of the 979 photon from the QM, which is crucial for quantum repeaters based on heralded entanglement and

feed forward. This experiment also fulfills milestone M2.9. Building on this experiment should allow distributing entanglement between remote quantum memories, with a greatly enhanced multimode capacity and correspondingly higher rates.

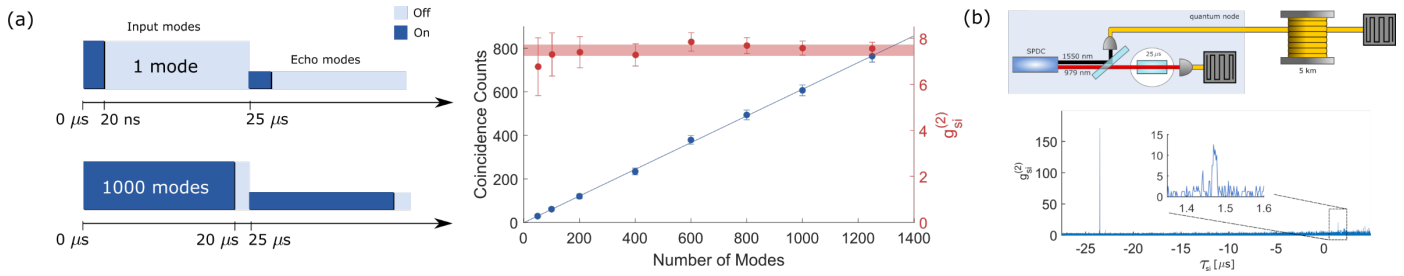


Fig. 5. a) Analysis of the multimode capacity by progressively increasing the number of modes included in the post-processing.

The mode size is 20 ns which entirely captures the correlation peak after storage. The value of $g_{si}^{(2)}$ is calculated by integrating over the full mode, which reduces to about half of the peak value (compare to Fig. 4). b) Measurement of the cross correlation after propagation of the telecom photon through a fiber spool of 5 km, where the telecom photon is detected 1.47 μ s before the release of the 979 nm photon from the Yb:YSO memory. This demonstrates remote distribution of non-classical correlations across 1250 temporal modes.

5.3 Thulium quantum memories (TUD)

TUD has demonstrated quantum correlations between a Tm:Y₃Ga₅O₁₂ (Tm:YGG) quantum memory, which allows storing 795 nm wavelength photons, and photons at telecommunication wavelength of 1532 nm⁹. Towards this end they created a source of photon pairs based on widely non-degenerate spontaneous parametric down-conversion of 523 nm laser pulses inside a periodically poled LiNbO₃ crystal. The resulting 1532 nm photons were directed through a few meters of standard telecom fiber to a superconducting nanowire single-photon detector (SNSPD), and their detections heralded the presence of 795 nm photons. The memory for the latter employed the two-level atomic frequency comb protocol—in this case using the transition between the lowest Stark levels of the ³H₆ and ³H₄ manifolds shown in the inset of Fig. 6—with fixed storage time.

After having verified proper operation of the memory, including the storage of laser pulses during up to 100 μ s, the heralded 795 nm photons were directed into, stored in, and released after 43 ns from the Tm:YGG memory (see Fig. 6 for the experimental setup related to the memory). The AFC bandwidth was tailored to 4 GHz to approximately match the photon bandwidth of 10 GHz (the remaining discrepancy induced more than 50% loss), and the magnetic field was set to 3 kG to match the difference in ground and excited state level splitting with the spacing between a trough and the neighboring tooth in the AFC. In addition, this choice resulted in tens' of seconds long AFC persistence, which allowed repeating the preparation sequence only every 10s. Together with the preparation time of 1s, this resulted in a memory

availability of around 90%. After re-emission, the photons were detected using a single-photon detector based on a silicon avalanche photodiode. The system efficiency, assessed by comparing photon detection rates with and without memory, was 0.05%. Taking 60% loss due to spectral mismatch between photon and memory bandwidth as well as 15% fiber coupling into account, this yields an internal storage efficiency after 43 ns storage of 0.85%. This currently small value can be increased by a factor of 20 by embedding the crystal inside an impedance-matched cavity. Additional improvements are expected after reducing spectral diffusion, in particular by using a more-stable magnetic field and a laser for AFC generation with better stability.

To verify that the non-classical correlations with the 1532 nm photons persist throughout the storage process, we measured the 2nd order cross-correlation coefficient $g^{(2)}_{12}(t)$ between the two photons of a pair using time-resolved coincidence detection. Before storage, we found $g^{(2)}_{12}(0) = 18 \pm 0.02$ and, importantly, after 43 ns storage $g^{(2)}_{12}(43 \text{ ns}) = 4.58 \pm 0.46$ (this value is reduced due to excess loss combined with detector dark counts). Both values surpass the classical upper bound of 2, confirming the quantum nature of the photon source as well as the memory. They are currently limited by the high brightness of the photon-pair source, chosen in this demonstration to increase the coincidence count rates.

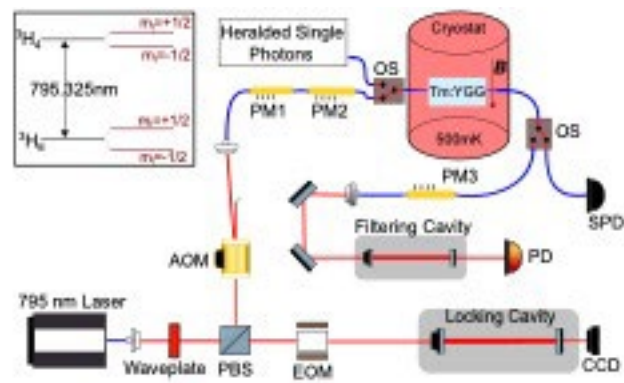


FIG. 6. Experimental setup. AOM: acousto-optic modulator; PM: phase modulator; OS: optical switch; EOM: electro-optic modulator; PD: Classical photo detector; SPD: Single photon detector; CCD: charge-coupled device camera; B: Magnetic field. Inset: Simplified energy level diagram of Tm:YGG showing the $^3\text{H}_6 \leftrightarrow ^3\text{H}_4$ zero-phonon line.

6. Non-classical correlations and entanglement between on-demand quantum memories and telecom photons

6.1 Emissive quantum memories and quantum frequency conversion

A very convenient method to directly generate light-matter entanglement in atomic ensembles is the Duan-Lukin-Cirac-Zoller (DLCZ) protocol¹⁰. It is based on the off-resonant excitation by means of weak classical write pulses of an atomic ensemble with a lambda system. With a small probability, a Raman scattered write photon creates a collective spin excitation, heralded by the emission of a Stokes photon. The spin wave can be converted into a second photon, the

anti-Stokes photon, with the use of a strong on-resonant read pulse. The DLCZ protocol has been very successfully implemented in cold atomic gases. However, the standard off resonant DLCZ scheme is difficult to apply to rare-earth ion doped crystals, due to the very weak dipole moments of the optical transition. Alternative schemes have been proposed that use resonant excitation and rephasing techniques to counteract the inhomogeneous dephasing of the atomic dipoles. ICFO and UNIGE have demonstrated a photon pair source with embedded quantum memory using a combination of the atomic frequency comb and the Duan-Lukin-Cirac-Zoller scheme using solid-state quantum memories based on a $\text{Pr}^{3+}:\text{Y}_2\text{SiO}_5$ and $\text{Eu}^{3+}:\text{Y}_2\text{SiO}_5$ crystal, respectively ICFO demonstrated entanglement between the photons, and UNIGE demonstrated a long storage time for non-classical correlations up to 20 ms. .

6.1.1 Entangled photon pair source in $\text{Pr}^{3+}:\text{Y}_2\text{SiO}_5$

ICFO has demonstrated a solid-state entangled photon pair source with an embedded quantum memory¹¹. In this source, the detection of a photon heralds the presence of a collective spin excitation in the quantum memory, which after a variable storage time can be read-out and converted into a single photon. This source has already been described in D 3.4, but we include it again here, as it is very relevant to the main goal of this deliverable.

ICFO's source is based on the combination of the atomic frequency comb and the Duan-Lukin-Cirac-Zoller scheme using a $\text{Pr}^{3+}:\text{Y}_2\text{SiO}_5$ crystal solid-state quantum memory. The experimental setup and the relevant level scheme is shown in Fig. 7. The write pulse is sent in resonance with the AFC created in the crystal. The detection of an initial Stokes photon heralds the presence of a single spin wave stored in the crystal, which can then be read-out on demand, emitting a single photon time-bin qubit. The retrieved single photon has a duration of 700 ns (FWHM), corresponding to a linewidth of 630 kHz.

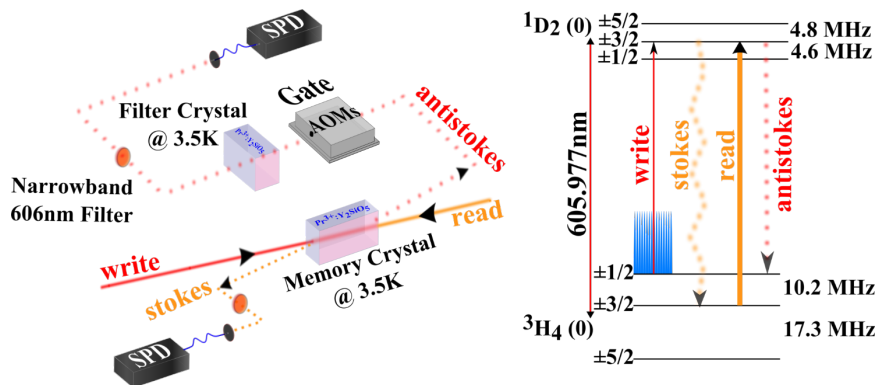


Figure 7. Left, Experimental setup. Right: Level scheme Pr:YSO

The source has been characterized by measuring the second-order cross-correlation function $g^2_{s,as}$, as a function of the probability to generate a Stokes photon (see Fig. 8). We reached $g^2_{s,as}$ values up to 20 for a coincidence window of 600 ns, strongly in the quantum regime. The coincidence count rate was increased by a factor of 8 compared to a

previous demonstration by ICFO¹². In addition, we have also demonstrated a violation of Bell inequalities with the emitted photons.

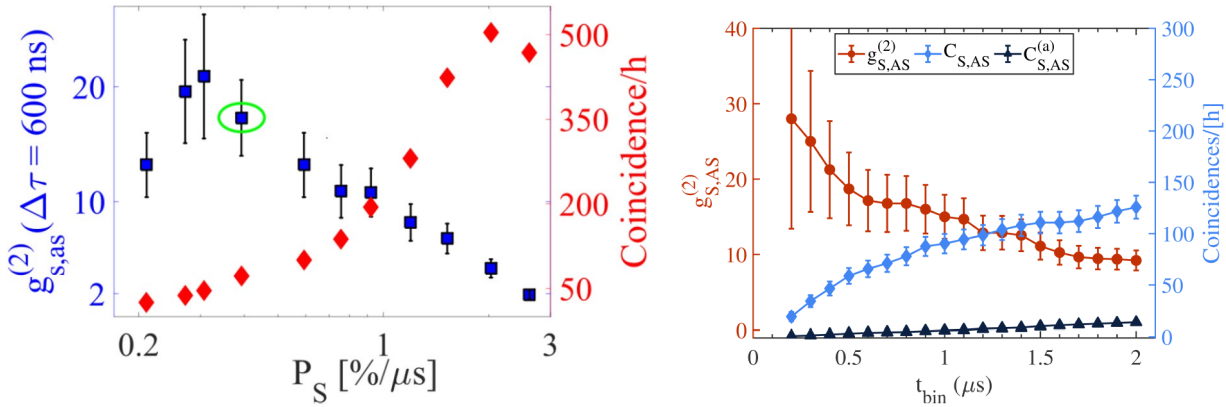


Figure 8. Left: Measurement of second order cross correlations (blue squares) and coincidence count rate (red diamond) for the photon pairs emitted by the quantum memory as a function of the probability to generate a Stokes photon. Right: Second order cross correlation (red), coincidences and accidental coincidences as a function of the coincidence detection window.

The read-out efficiency is currently of the order of 2 %. This value could be increased by suppressing background noise in the Stokes photon emission, by improving the AFC preparation, by a better control of the spin decoherence as well as by using a longer crystal with higher optical depth and/or by embedding the crystal in a low finesse cavity¹³. Furthermore, background noise suppression would also allow us to widen the coincidence window, leading to a higher coincidence rate, as shown in Fig. 8.

We have designed and built a cavity, which is now operative and incorporated in our memory setup, and we have recently improved the efficiency of an excited state AFC quantum memory up to 62 %, the highest value measured so far for an AFC memory¹⁴ (for a more detailed description, see Deliverable D2.1). Investigations are ongoing to extend cavity enhanced storage to spin-waves and we also plan to combine the impedance matched cavity with AFC-DLCZ generation.

Sources using emissive quantum memories emit photons resonant with the optical transition of the ions, in our case at 606 nm. It is then necessary to convert them to telecom wavelength to be used in a long distance quantum repeater link. ICFO has implemented quantum frequency conversion with weak coherent states mimicking the single photons emitted by the quantum memory, using difference frequency generation with a strong pump beam at 994 nm, in a periodically poled lithium niobate waveguide. We have achieved quantum frequency conversion of weak pulses with duration 700 ns with a total device efficiency of 21.5%, and a μ_1 value of $4.3 \cdot 10^{-3}$ (mean number of photons at the input to achieve a signal-to noise ratio at the output of 1), which would allow a conversion with SNR around 4.6 for the single

photons emitted by the quantum memory, even with the currently low read-out efficiency. More details on the QFC are available in Deliverable D3.4. Measurements to improve the signal to noise ratio are under way.

6.1.2 Long-lived photon pair source in $\text{Eu}^{3+}:\text{Y}_2\text{SiO}_5$

The group at UNIGE has been performing a similar experiment based on Europium-doped Y_2SiO_5 , with the addition of a dynamical decoupling sequence to reach storage times between 20 and 100 ms. Some basic characteristics of the memory device were characterized using weak coherent states at the single-photon level, as described in Ortu et al.¹⁵. This led to the benchmark for fidelity of 85% for the storage of a time-bin qubit and to the record for the highest storage time of a quantum state in a solid state-based absorptive photonic quantum memory of 20ms.

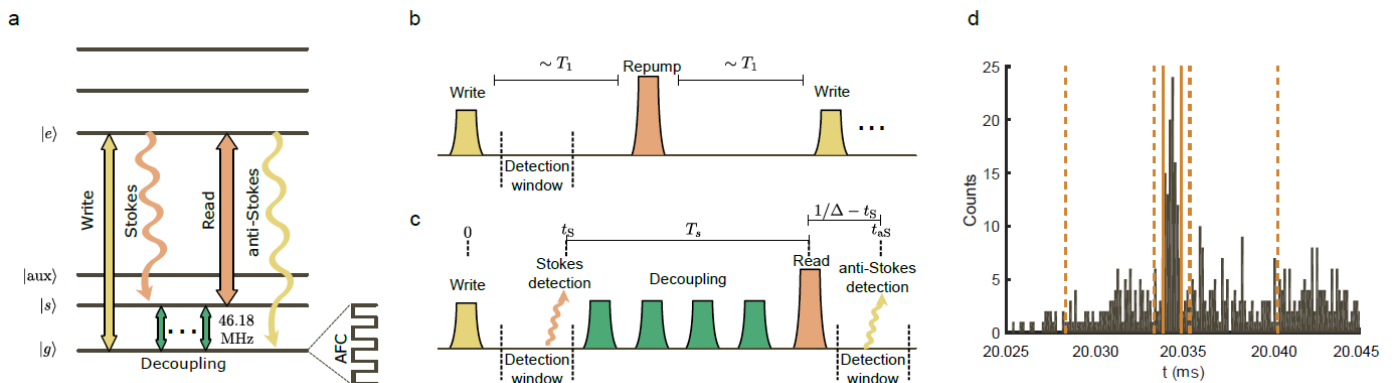


Figure 9. (a) Energy level diagram showing the relevant transitions used in the DLCZ experiment. (b) "Write mode" where up to 50 Write pulses are applied with a 10 ms delay. (c) Conditioned on the detection of a Stokes photon in the detection gate following a Write pulse, the "storage mode" sequence is applied. (d) Example of a coincidence histogram between Stokes and anti-Stokes photons.

Our approach allows us to transfer the same properties into an integrated photon source and memory device in a DLCZ-like setup.

To increase its repetition rate, the experiment was done in a conditional mode. Hence, in the case of no recorded Stokes detection a repump pulse was applied to empty the $|s\rangle$ state and then another Write pulse was applied, see Fig. 9b. In the case a Stokes photon was detected, fast FPGA electronics switched to a "storage mode" where the spin-wave was manipulated by a dynamical decoupling RF sequence, followed by an optical Read pulse to convert the single spin excitation to a single anti-Stokes photon, see Fig.9c. The dynamics of the AFC assures that a strong collective emission of the anti-Stokes is time-correlated with the detection of the Stokes photon. This time-correlation provides a multi-mode DLCZ scheme. An example of coincidence measurement between Stokes and anti-Stokes detections is shown

in Fig.4d, where the storage time in the quantum node was 20 ms. The measured second-order cross correlation function was $g_{si} = 5.02 \pm 0.69$, for a bin size of $T_b = 1 \mu\text{s}$. Given a detection window of $10 \mu\text{s}$ and a bin size of $1 \mu\text{s}$, it follows that the non-classical correlations were generated over 10 temporal modes.

The probability to generate a Stokes photon in a single temporal mode of duration T_b inside the $\text{Eu:Y}_2\text{SiO}_5$ crystal was $6.3 \cdot 10^{-3}$, which corresponds to the pair production probability p of a conventional SPDC source. In the total detection gate the Stokes generation probability was then 6.3%, but given the crystal-to-detector transmission of 18% and the detection probability of 56%, the Stokes detection probability per gate was $6.4 \cdot 10^{-3}$. Taking into account the 50 repetitions it follows that there was a 32% probability to detect a heralding photon over 500 ms, which translates to about 0.6 Hz heralding rate. The main limitation in the heralding rate is the low crystal-to-detector transmission and the repump duration of 10 ms.

The read-out efficiency of the anti-Stokes photon was evaluated from the coincidence histogram in Fig. 4d, which resulted in $(3.6 \pm 0.4)\%$. The efficiency is much smaller than expected both from the theory and the characterization published in Ortu et al.¹⁵. Indeed, a DLCZ-type operation of a memory node is expected to be larger than the corresponding read-write storage, as in DLCZ operation only the read-out efficiency enters, while in read-write operation both the write (absorption) and read out efficiency enters. The read-write efficiency was 7.4%, from which we expected an efficiency in the range of 10-15% in DLCZ operation. This discrepancy is not understood at this point. The major points that need improvement in the current set-up is the crystal-to-detector transmission, the low read-out efficiency and the noise induced by the Read pulse.

In parallel, UNIGE has worked on a quantum frequency converter (QFC), to convert the 580 nm Stokes photons into the 1550 telecom band. In the current QFC setup, improved from the one described in Ref. ¹⁶, we obtain a maximum of 20 % total efficiency from the input 580 nm fiber to the output 1550 nm fiber, including the narrow band noise filter. The noise level of the converter is below 10 Hz, obtained by filtering the QFC output through a frequency-locked optical cavity with 6.3 MHz bandwidth. As the QFC will replace our current crystal-to-detector path on the Stokes mode, with a similar efficiency, we expect similar coincidence rates and cross correlation values after the QFC, but with the ability to generate remote non-classical correlations with a 20 ms quantum memory.

6.2 Absorptive quantum memories

ICFO demonstrated entanglement between a photon at telecom wavelength and a solid-state on-demand quantum memory based on Pr:YSO ⁵. As mentioned in sec. 5.1, on-demand read-out from the Pr-ions can be implemented with the full AFC protocol. In this case, after a photon is absorbed by the AFC a strong optical pulse transfers the collective excitation to a ground spin state, where the re-phasing process is effectively frozen, until a second optical control pulse recalls it back to the excited state. The time between the two control pulses can be changed at will, therefore introducing on-demand read-out of the stored photon, at the cost of a reduced storage efficiency η_{sw} . This can be expressed as

$\eta_{SW} = \eta_{AFC} \eta_T^2 \eta_C$, where η_{AFC} is the efficiency of the AFC storage, η_T is the efficiency of the control pulses in transferring the population to and from the spin states, and η_C is an efficiency term due to the spin inhomogeneity of the Pr ions. It causes a decrease in storage efficiency for increasing storage in the spin state, and it can be expressed as $\eta_C = \exp(-\frac{(T_S \gamma_{inhom} \pi)^2}{2 \log(2)})$, where T_S is the storage time in the spin state and γ_{inhom} is the width of the spin inhomogeneous broadening. Storage in the spin wave causes also an decrease in the signal-to-noise ratio, due to fluorescence from the strong control pulses. Careful control of the population of the ion and a narrow filtering of the noise is therefore required.

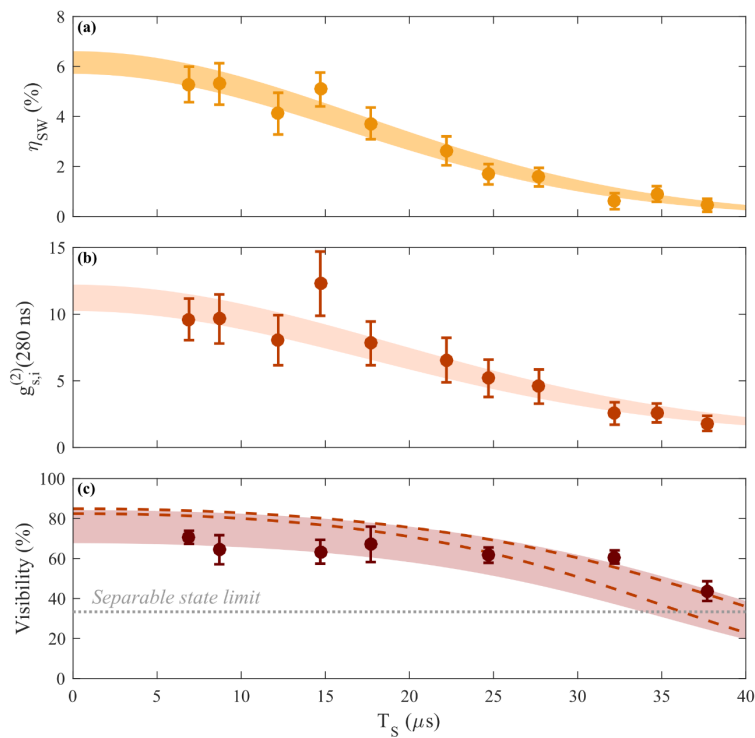


Figure 10: (a) storage efficiency, (b) cross-correlation function and (c) visibility of interference as a function of storage time in the spin state. The shaded area for (a) and (b) represent a variation of one sigma from the fit, from which we calculated the spin inhomogeneous broadening. The shaded area for (c) similarly is one sigma of error from a fit, that instead account for the expected visibility at each storage time. A detailed description of the model is reported in Ref. [5].

We characterised the system in a similar manner as for fixed-delay AFC, by measuring the storage efficiency and the cross-correlation between the telecom idler photon and the retrieved spin-wave excitation, this time for a storage in the AFC of 10 μs and for varying storage in the spin state⁵. The results are reported in Fig. 10(a) and (b), where we report non-classical correlations up to a T_S of 37.5 μs . From the data we also extracted a spin inhomogeneous broadening of 16.1(7) kHz. For the entanglement analysis, we perform a similar experiment as for sec. 5.1, with the difference that we now prepare in the filter crystal only one AFC with a storage of 420 ns, and the two delays of the interferometer are represented by storage in the AFC and by transmission through it. The results are reported in Fig. 10(c), where we demonstrate a visibility above the classical limit of 33% for all the cases considered. For the shortest measured storage time, we obtain a two qubit fidelity of 77 (2) % with respect to a maximally entangled state.

7. Telecom heralded entanglement between remote solid-state multiplexed quantum memories

The realisation of telecom-heralded entanglement between remote multimode quantum memories is the cornerstone of several promising architectures for a quantum network. The distribution of entanglement between remote nodes allows the exchange of quantum information through quantum teleportation, but only in a heralded fashion can it reach its full potential, without the need of post-selection. The compatibility of the heralding signal with the telecom network is also a coveted property, since it will allow the use of deployed commercial fibres with low-loss transmission. Multimodality is equally important, since without it the maximum rate at which entanglement can be attempted is given by the communication time: a separation of 100 km would correspond to a maximum rate of 2 kHz. In this direction, ICFO demonstrated the entanglement of two Pr-based quantum memories separated by 10m and heralded by a telecom photon¹⁷.

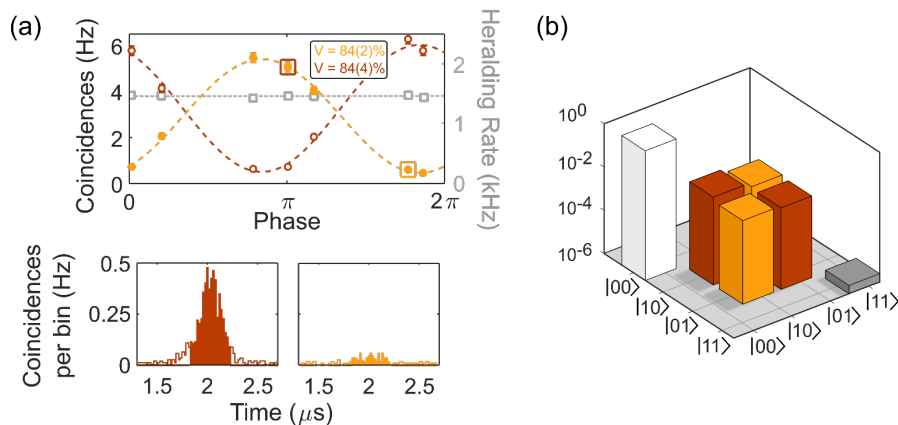


Figure 11: (a) Interference fringes obtained at the two outputs of the beamsplitter by recombining the two signal modes (circles) and heralding rate (squares). Each point was obtained by integrating for about 2 min, and with a coincidence window of 400 ns. The two bottom plots represent the actual coincidence histograms for the points indicated in the fringe plot. (b) Reconstructed density matrix for the matter–matter entangled state of the two remote quantum memories.

The system is the same described in Sec. 5.1, that was duplicated for this experiment. The idler photons from two SPDC sources were collected in single mode optical fibres, that were then crossed at a fibre beam splitter. This erases the which-path information of the idler photons, such that a detection event after the beam splitter heralds the generation of an entangled state of the two quantum memories, that share one signal photon as a delocalised excitation. The entanglement was then verified by performing a full tomography of the state, and calculating the concurrence from the retrieved density matrix. An initial test was performed, with a 2 us AFC prepared in each quantum memory (see Fig 11). The heralding rate was 1.4 kHz, a record value for heralded entanglement between solid-state quantum memories, and

the photon purity $h_c^{(2)}$ was less than 4%. From the density matrix we extracted a concurrence of $1.15(5) \cdot 10^{-2}$, which is positive by more than 20 standard deviation, and therefore a definitive confirmation of the non-classical correlations between the two quantum memories. The high contribution of the vacuum component to the density matrix, visible in Fig. 11(b), is mostly due to the various losses in the signal channels. It can be reduced by back-tracing the value of the concurrence to the crystal: the concurrence is then rescaled to $7.3(5) \cdot 10^{-1}$ that is still limited mostly by the source heralding efficiencies and to a lesser extent by the imperfect visibility and memory-write efficiencies. Moreover, in a Duan–Lukin–Cirac–Zoller (DLCZ)-like quantum repeater with built-in purification the vacuum component would only affect the entanglement distribution rate but not the fidelity of the repeater. To provide an estimation of how well our entangled link would perform in such a repeater we defined an effective fidelity considering only the one- and two-photon terms of the matrix, and we inferred values of fidelity to ideal state of 92(1)%.

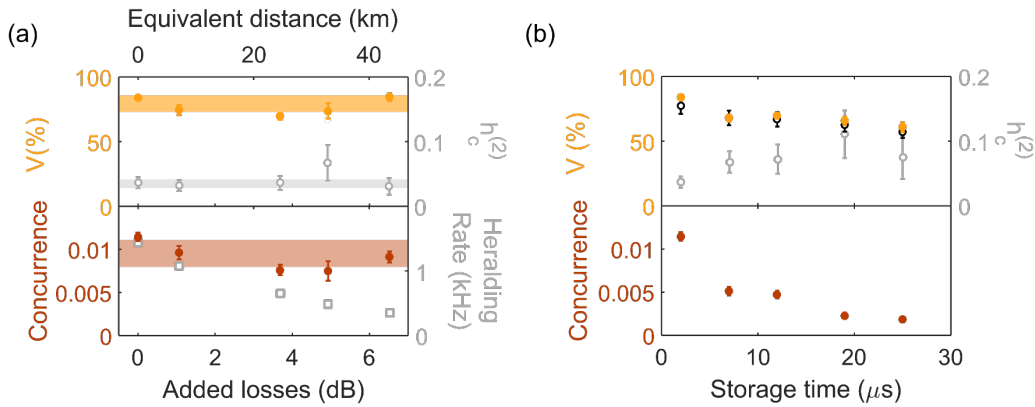


Figure 12: (a) Increasing losses in the idler channels. Although the heralding rate decreases, the concurrence remains constant. The error bars represent one standard deviation. **(b)** Increasing storage time. We increased τ up to 25 μs , and measured positive concurrence for all cases. The empty dark circles are the expected values for visibilities, and the error bars represent one standard deviation.

This type of entanglement is particularly suitable to long distance communication, since any additional loss on the idler paths would only result in a decrease in the entanglement heralding rate, but not in the quality of the entanglement. To demonstrate this, we introduced variable attenuators on both idler paths, introducing losses equivalent to a propagation in fibre of up to 40 km (7 dB). For all points we measured the concurrence again, which remained constant and positive for all acquired data (see Fig. 12.a). The heralding rate is instead decreasing, as expected. Next, we extended the storage time of the quantum memory to up to 25 μs , and measured again the concurrence. As visible in Fig. 12(b) we measured positive concurrence for all cases, despite it decreased for increasing storage time, due to the decreasing efficiency of the AFC storage. Moreover, the longest storage time of 25 μs allows for the storage of 62 distinct temporal modes, which translates directly into an increase of a factor of 62 in the heralding rate with respect to a single mode equivalent system, in case of quantum memories separated by more than 5 km (corresponding to a communication time of 25 μs).

8. Conclusion

In this report, we described the progress realized during QIA towards the realization of memory based quantum repeaters. We have made significant progress in experiments demonstrating entanglement and non-classical correlations between telecom photons and solid-state quantum memories. We have also reported the first demonstration of telecom heralded entanglement between multimode quantum memories, that can in principle be extended to long distances.

For light-matter entanglement and quantum correlations in fixed storage time solid-state quantum memories, we used external non-degenerate photon pair sources where one photon is resonant with the quantum memory and the other photon is at telecommunication wavelengths. We have increased the entanglement storage time by more than two orders of magnitude compared to the state of the art before QIA. The temporally multimode capacity for non-classical correlations was increased by more than one order of magnitude, leading to a world record of number of modes stored in a quantum memory. We have also demonstrated light-matter quantum correlations with a quantum memory that will allow massive frequency multiplexing. Finally, we have demonstrated long distance entanglement and quantum correlations, including over up to 50 km of installed optical fiber in the Barcelona area.

For on-demand quantum memories, we used two approaches to generate light-matter quantum correlations and entanglement. The first is an extension of the non-degenerate photon pair source used for fixed storage time memories, but now with transfer of the stored qubit to spin states in the quantum memory. We have reported the first demonstration of entanglement between a telecom photon and a multimode solid-state quantum memory. The second approach is to use the quantum memory as source of correlated and entangled photons. We have reported the first demonstration of light-matter entanglement in solid-state quantum memories using that technique, as well as long-lived (up to 20 ms) quantum memory light-matter quantum correlations. While large values of cross-correlations have been achieved (up to 20), the retrieval efficiency was limited to a few percents, which led to low count rates. More progress is needed before this approach can be incorporated in an elementary quantum repeater link. Also, the feasibility of the required quantum frequency conversion has been demonstrated with weak-coherent pulses, although the conversion of the quantum light emitted from the quantum memory has not been achieved yet.

Finally, we have reported the first demonstration of telecom heralded entanglement between multimode quantum memories that can in principle be extended to long distances. Each quantum node was composed by a non-degenerate photon pair source and a solid-state quantum memory. The two quantum memories were placed in two different laboratories located 10m apart. We used a single photon detection Bell State measurement that projected the two quantum memories in an entangled state in the Fock basis. This led to a record heralding rate of up to 1.4 kHz, together with a 92 % effective fidelity, limited by the available pump power for the sources. We also demonstrated multiplexed enhanced entanglement with up to 62 temporal modes, as well as the demonstration that the scheme can tolerate loss in the heralding arms equivalent to up to 40 km optical fiber distance. The approach demonstrated is directly extendable over longer distances and ICFO is preparing an experiment over tens of km of optical fibers. The next challenges in

that direction are increasing the storage time to hundreds of microseconds (longer than the communication time), which will be achieved by using spin-wave storage and spin-echo techniques similar to the one that have been demonstrated by UNIGE, implement phase stabilization over the long fiber link (which has been achieved in QIA using the prototype developed by MuQuans, but still needs to be adapted to our experiment) and increase the multimodality of the memory, e.g. by adding spectral and spatial multiplexing.

9. References

-
- ¹ M. Afzelius, C. Simon, H. de Riedmatten and N. Gisin, Phys. Rev. A 79, 052329 (2009).
 - ² A. Seri, D. Lago-Rivera, A. Lenhard, G. Corrielli, R. Osellame, M. Mazzera and H. de Riedmatten, Phys. Rev. Lett. 123, 080502 (2019).
 - ³ P. Jobez, N. Timoney, C. Laplane, J. Etesse, A. Ferrier, P. Goldner, N. Gisin and M. Afzelius, Phys. Rev. A, 93, 032327 (2016).
 - ⁴ J. D. Franson, Phys. Rev. Lett. 62, 2205 (1989).
 - ⁵ J. V. Rakonjac, D. Lago-Rivera, A. Seri, M. Mazzera, S. Grandi and H. de Riedmatten, Phys. Rev. Lett. 127, 210502 (2021).
 - ⁶ A. Ortu, A. Tiranov, S. Welinski, F. Fröwis, N. Gisin, A. Ferrier, P. Goldner, and M. Afzelius, Nature Materials 17, 671 (2018)
 - ⁷ M. Businger, A. Tiranov, K. T. Kaczmarek, S. Welinski, Z. Zhang, A. Ferrier, P. Goldner, and M. Afzelius, Phys. Rev. Lett. 124, 053606 (2020).
 - ⁸ S. Welinski, A. Tiranov, M. Businger, A. Ferrier, M. Afzelius, and P. Goldner, Phys. Rev. X 10, 031060 (2020)
 - ⁹ M. Falamarzi Askarani *et al.*, Phys. Rev. Lett. 127, 220502 (2021).
 - ¹⁰ L.M. Duan, M. Lukin, J.I. Cirac and P. Zoller, Nature 414, 413 (2001).
 - ¹¹ K. Kutluer, E. Distanti, B. Casabone, S. Duranti, M. Mazzera, and H. de Riedmatten, Phys. Rev. Lett. 123, 030501 (2019).
 - ¹² K. Kutluer, M. Mazzera, and H. de Riedmatten Phys. Rev. Lett. 118, 210502 (2017).
 - ¹³ M. Afzelius and C. Simon, Phys. Rev. A 82, 022310 (2010).
 - ¹⁴ S. Duranti, S. Wengerowski, A.Seri, B.Casabone, H.de Riedmatten, in preparation (2022).
 - ¹⁵ A. Ortu, A. Holzäpfel, J. Etesse, and M. Afzelius, npj Quantum Inf.8, 29 (2022)
 - ¹⁶ P. Strassmann, A. Martin, N. Gisin, and M.Afzelius, Opt. Express 27, 14298 (2019)
 - ¹⁷ D. Lago-Rivera, S. Grandi, J. V. Rakonjac, A. Seri and H. de Riedmatten, Nature 594, 37-40 (2021).